Protons and alpha particles in the expanding solar wind: Hybrid simulations

Petr Hellinger[1,2] and Pavel M. Trávníček[3,1,2]

Abstract. We present results of a two-dimensional hybrid expanding box simulation of a plasma system with three ion populations, beam and core protons, and alpha particles (and fluid electrons), drifting with respect to each other. The expansion with a strictly radial magnetic field leads to a decrease of the ion perpendicular to parallel temperature ratios as well as to an increase of the ratio between the ion relative velocities and the local Alfvén velocity creating a free energy for many different instabilities. The system is most of the time marginally stable with respect to kinetic instabilities mainly due to the ion relative velocities; these instabilities determine the system evolution counteracting some effects of the expansion. Nonlinear evolution of these instabilities leads to large modifications of the ion velocity distribution functions. The beam protons and alpha particles are decelerated with respect to the core protons and all the populations are cooled in the parallel direction and heated in the perpendicular one. On the macroscopic level the kinetic instabilities cause large departures of the system evolution from the double adiabatic prediction and lead to perpendicular heating and parallel cooling rates which are comparable to the heating rates estimated from the Helios observations.

1. Introduction

In the solar wind the proton and alpha particle temperatures decrease with the radial distance R slower than what is expected from the adiabatic prediction $\propto R^{-4/3}$ [*Marsch et al.*, 1982a, b]. Assuming a model which takes into account nonnegligible proton temperature anisotropies in the solar wind [*Hellinger et al.*, 2006], Helios observations indicate that in the parallel direction protons need to be cooled around 0.3 AU but further away they need to be heated whereas they need to be heated in the perpendicular direction (as well as in total) from 0.3 to 1 AU [*Hellinger et al.*, 2011, 2013]; the parallel and perpendicular heating (cooling) rates are comparable and are important fractions of the dimensional heating rate given as the ratio between the proton kinetic energy and the expansion time

$$Q_E = \frac{n_{\rm p} k_B T_{\rm p} v_{sw}}{R}. \quad (1)$$

[cf., *Vasquez et al.*, 2007]; for symbol definition see Appendix.

On the microscopic level the proton velocity distribution function typically consists of two populations, core and beam [*Marsch et al.*, 1982b], which decelerate with respect to each other following roughly the local Alvén velocity. This deceleration is related to the proton parallel cooling. Alpha particles also sometimes exhibit two populations and decelerate with respect to the core protons following roughly the local Alvén velocity [*Marsch et al.*, 1982a]. The alpha particle (and proton beam) kinetic energy being lost during this deceleration likely contributes to ion heating [*Schwartz et al.*, 1981; *Schwartz and Marsch*, 1983].

Ulysses observations of alpha particles in the fast, high-latitude solar wind [*Reisenfeld et al.*, 2001] indicate that alpha particles need to be heated in total (but they need to be cooled in the parallel direction) and the necessary heating rate matches the energy lost due to the relative alpha-proton deceleration.

Physical mechanisms responsible for the observed evolution of ion thermal energetics (and of their velocity distribution functions) are yet to be determined; different mechanisms are expected to be relevant at different radial distances and for different solar wind plasma parameters; furthermore, multiple phenomena may coexist and compete with each other. The solar wind rotation influences the differential ion-ion velocities [*McKenzie et al.*, 1979; *Hollweg and Isenberg*, 1981]. The azimuthal (transverse) particle velocity components importantly affect the radial momentum transport in the solar wind leading to the relative deceleration between alpha particles and protons [*Li et al.*, 2007]; this effect, however, does not seem to account for the observed relative deceleration in the fast solar wind between 0.3 and 1 AU but may be relevant for the Ulysses observations [*Li et al.*, 2007].

The Coulomb collisions naturally reduce the differential velocities between different species [*Neugebauer*, 1976; *Kasper et al.*, 2008] and contribute to a (possible differential) particle energization [*Matteini et al.*, 2012]. While the Coulomb collisions are relevant in slow solar wind streams, fast solar wind streams are essentially collisionless. In collisionless plasmas interactions between ions and electromagnetic fluctuations (magnetohydrodynamic turbulence and/or waves) are the usual suspects.

The role of the magnetohydrodynamic turbulence in the solar wind and its effect on the particle energetics and velocity distribution function remain an open question [*Matthaeus and Velli*, 2011]. Estimations based on the stationary Kolmogorov-Yaglom law [e.g., *MacBride et al.*, 2008] indicate that there is enough energy in the turbulent cascade to heat protons. However, the stationarity assumption in the expanding solar wind is questionable [*Hellinger et al.*, 2013]. Interactions between ions and (parallel propagating) Alfvén/ion cyclotron waves is another relevant mechanism which may influence properties of protons and alpha particles [*Liewer et al.*, 2001; *Hellinger et al.*, 2005]. Observations at 1 AU [*Kasper et al.*, 2008, 2013] indicate nontrivial correlations between ion parameters compatible with some of the expected properties of the cyclotron wave-particle interactions.

Ion temperature anisotropies and differential velocities are constrained by kinetic instabilities. Signatures of temperature-anisotropy driven instabilities are clearly observed in the solar wind [*Gary et al.*, 2001; *Hellinger et al.*, 2006; *Matteini et al.*, 2007; *Maruca et al.*, 2012] and signatures of instabilities driven by differential velocity between ion species [*Daughton and Gary*, 1998; *Verscharen et al.*, 2013] are also observed [*Marsch and Livi*, 1987; *Tu et al.*, 2004; *Goldstein et al.*, 2000; *Matteini et al.*, 2013]. It is unclear what are the relations between a magnetohydrodynamic

[1]Astronomical Institute, AS CR, Prague, Czech Republic
[2]Institute of Atmospheric Physics, AS CR, Prague, Czech Republic
[3]SSL, UC Berkeley, USA

0148-0227/13/2013JA019013$9.00

turbulence and/or important wave activity and kinetic instabilities (which are usually investigated in the approximation of homogeneous plasma and uniform magnetic field). However, observations of proton temperature-anisotropy bounds [*Hellinger et al.*, 2006] and enhanced magnetic fluctuations in the vicinity of theoretical marginal stability regions due to proton temperature-anisotropy driven instabilities [*Bale et al.*, 2009] indicate that these instabilities coexist with the magnetohydrodynamic turbulence/wave activity present in the solar wind. The beam-core and alpha particle-core relative velocity driven instabilities naturally reduce the relative velocities as a part of the saturation mechanism [*Daughton et al.*, 1999] and may be responsible for the deceleration of beam protons and alpha particles with respect to core protons and may contribute to ion energization [*Hellinger et al.*, 2003]. *Hellinger and Trávníček* [2011] (referred hereafter as Paper 1) used a hybrid expanding box model (which self-consistently models the competition between the expansion and ion kinetic instabilities) to investigate an evolution of a proton beam-core system in the expanding box. The hybrid expanding box simulation results indicate that kinetic instabilities driven by the beam-core relative velocity reduce this source of free energy leading to a parallel cooling and perpendicular heating in qualitative agreement with the observations. Further analysis [*Hellinger et al.*, 2013] indicates that the heating/cooling rates in the hybrid expanding box simulation due to the kinetic instabilities are comparable to the heating rates estimated from the Helios data indicating that the observed proton parallel cooling is caused by kinetic instabilities driven by the beam-core relative velocity.

In Paper 1 alpha particles were not included in the plasma model. This is rectified in this paper where we investigate the evolution of a more realistic plasma system consisting of proton core and beam populations, and of alpha particles drifting with respect to each other using the hybrid expanding box model. This paper is organized as follows, section 2 presents the numerical model (subsection 2.1) and its results concerning the evolution of waves and ions (subsection 2.2) and we calculate the heating rates in the simulated system (subsection 2.3). In section 3 we discuss the simulation results and compare them with observations.

2. Simulation results

2.1. Model and initial conditions

In this paper we use the Hybrid Expanding Box (HEB) model to study self-consistently the response of the solar wind plasma to a slow expansion [*Matteini et al.*, 2006; *Hellinger and Trávníček*, 2008]. In the HEB model the expansion is described as an external force where a constant solar wind radial velocity v_{sw} is assumed. The radial distance R is then

$$R = R_0 + v_{sw}t = R_0\left(1 + \frac{t}{t_{e0}}\right) \tag{2}$$

where R_0 is an initial radial distance and $t_{e0} = R_0/v_{sw}$ is the characteristic (initial) expansion time. Transverse scales (with respect to the radial direction) of a small portion of plasma, co-moving with the solar wind velocity, increase with time $\propto (1 + t/t_{e0})$. The expanding box uses these co-moving coordinates, replacing the spatial dependence by the temporal one (see Equation (2)). The physical transverse scales of the simulation box increase with time [see *Hellinger and Trávníček*, 2005, for a detailed description of the code].

The kinetic model uses the hybrid approximation, electrons are considered as a massless, charge neutralizing fluid, with a constant temperature; ions are described by a particle-in-cell model and are advanced by a Boris' scheme that requires the fields to be known at half time steps ahead of the particle velocities. This is achieved by advancing the current density to this time step with only one computational pass through the particle data at each time step [*Matthews*, 1994]. The characteristic spatial and temporal units used in the model are $v_A/\omega_{\mathrm{cp}0}$ and $1/\omega_{\mathrm{cp}0}$, respectively (for the definitions of symbols used here see Appendix. We use the spatial resolution $\Delta x = \Delta y = v_A/\omega_{\mathrm{cp}0}$, and there are $2,048$ particles per cell for the core protons and $1,024$ particles per cell for the proton beam as well as for alpha particles. Fields and moments are defined on a 2-D x–y grid with dimensions 512×512 with the periodic boundary conditions. Ions are advances with a time step $\Delta t = 0.05/\omega_{\mathrm{cp}0}$, while the magnetic field $\boldsymbol{B}$ is advanced with a smaller time step $\Delta t_B = \Delta t/10$. The initial ambient magnetic field is directed along the radial, x direction, $\boldsymbol{B}_0 = (B_0, 0, 0)$ and we impose a continuous expansion in the transverse (y and z) directions. For simplicity we here only consider a strictly radial magnetic field. In this case the expansion leads to a decrease of the ambient density and magnitude of the magnetic field as

$$n \propto B \propto \left(1 + \frac{t}{t_{e0}}\right)^{-2} \tag{3}$$

and the double adiabatic prediction of the proton temperature anisotropy and parallel beta in the expanding box is

$$\frac{T_{\mathrm{s}\parallel}}{T_{\mathrm{s}\perp}} \propto \beta_{\mathrm{s}\parallel} \propto \left(1 + \frac{t}{t_{e0}}\right)^{2}. \tag{4}$$

The expansion tends to increase $T_{\mathrm{s}\parallel}/T_{\mathrm{s}\perp}$ leading to the corresponding temperature anisotropy driven instabilities. Furthermore, the Alfvén velocity decreases $v_A \propto 1/(1 + t/t_{e0})$ whereas the parallel differential velocity v_{bc} between the proton core and beam populations is constant (for the strictly radial magnetic field) when no wave activity or collisions are present. This results in a continuous increase of their ratio,

$$\frac{v_{\mathrm{bc}}}{v_A} \propto 1 + \frac{t}{t_{e0}}, \tag{5}$$

which leads to beam driven instabilities.

For initial conditions we took these proton parameters:

$$\begin{aligned} &n_{\mathrm{c}} = 0.8n_{\mathrm{e}},\ n_{\mathrm{b}} = 0.1n_{\mathrm{e}},\ v_{\mathrm{bc}} = 1.3v_A, \\ &\beta_{\mathrm{p}\parallel} = 0.2,\ \beta_{\mathrm{b}\parallel} = 0.1,\ T_{\mathrm{c}\perp}/T_{\mathrm{c}\parallel} = 1.8,\ T_{\mathrm{b}\perp}/T_{\mathrm{b}\parallel} = 1 \end{aligned} \tag{6}$$

while for alpha particles we set

$$\begin{aligned} n_\alpha = 0.05n_{\mathrm{e}},\ v_{\alpha\mathrm{c}} = 0.8v_A, \\ \beta_{\alpha\parallel} = 0.05,\ T_{\alpha\perp}/T_{\alpha\parallel} = 1. \end{aligned} \tag{7}$$

The characteristic time was chosen to be $t_{e0} = 10^4/\omega_{\mathrm{cp}0}$, which is about 10 times faster than in the solar wind. We chose these parameters for comparison with Paper 1 where similar proton parameters were used.

2.2. Waves, particles and instabilities

The chosen initial conditions are stable with respect to kinetic instabilities. The expansion, however, tends to change the plasma properties which typically create a free energy for kinetic instabilities. Let us investigate the evolution of the HEB simulation starting with the wave activity. Figure 1 displays the evolution of the magnetic fluctuations. The top panel shows the fluctuating magnetic field $\delta B^2/B_0^2$ as a function of time. The other two panels display gray scale plots of the fluctuating magnetic field δB as a function of time and wave vector k (middle panel) and as a function of time and propagation angle θ_{kB} (bottom panel). Figure 1 shows that initially there is no important wave energy in the system. At about $0.1t_{e0}$ electromagnetic waves start to appear around the parallel propagation with wavevectors $0.5 \lesssim kv_A/\omega_{\mathrm{cp}} \lesssim 1$. At about $0.4t_{e0}$ oblique waves with the angle of propagation $\theta_{kB} \sim 45^{\mathrm{o}}$ and wavevectors $k \sim 0.1\omega_{\mathrm{cp}}/v_A$. These oblique waves appear in a transient manner (reminding the self-destructive properties of the oblique fire hose instability). As the oblique waves appear and disappear the relative fluctuating magnetic energy $\delta B^2/B_0^2$ decreases. Later on, $\delta B^2/B_0^2$ increases with time again.

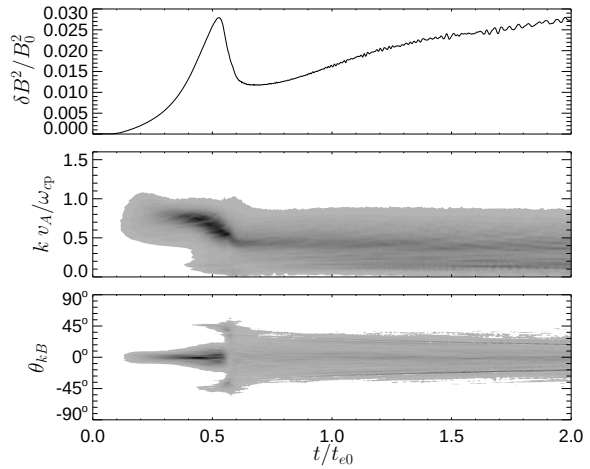

Figure 1. Evolution of the magnetic fluctuations: (top) Fluctuating magnetic field $\delta B^2/B_0^2$ as a function of time. Gray scale plots of the fluctuating magnetic field δB as a function of time and wave vector k (middle panel) and as a function of time and propagation angle θ_{kB} (bottom panel).

A similar evolution is also seen in the proton density fluctuations. Figure 2 displays the evolution of the proton density fluctuations in the HEB simulation in the same format as in Figure 1. The top panel shows the proton density fluctuations $\delta n_{\rm p}^2/n_{\rm p0}^2$ The middle and bottom panels display gray scale plots of proton density fluctuations $\delta n_{\rm p}$ as a function of time and wave vector k and as a function of time and propagation angle θ_{kB}, respectively.

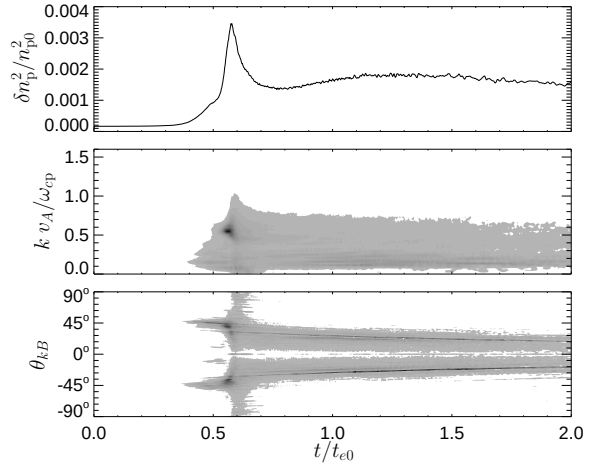

Figure 2. Evolution of the proton density fluctuations: (top) Proton density fluctuations $\delta n_{\rm p}^2/n_{\rm p0}^2$ as a function of time. Gray scale plots of the proton density fluctuations $\delta n_{\rm p}$ as a function of time and wave vector k (middle panel) and as a function of time and propagation angle θ_{kB} (bottom panel).

The density fluctuations are not seen for the nearly parallel propagating waves in agreement with the linear expectations whereas at more oblique angles the evolution of the density fluctuations is similar to that of the magnetic fluctuations.

The interaction between waves and ions leads to important modifications of the ion velocity distribution functions. Figure 3 shows the proton (left panels) and alpha particle (right panels) velocity distribution functions as functions of $v_\parallel$ and $v_\perp$ at (top panels) $t = 0.4t_{e0}$, (middle upper panels) $t = 0.5t_{e0}$, (middle lower panels) $t = 0.6t_{e0}$ and (bottom panels) at $t = 2t_{e0}$. The overplotted dashed lines displays the local Alfvén velocity v_A.

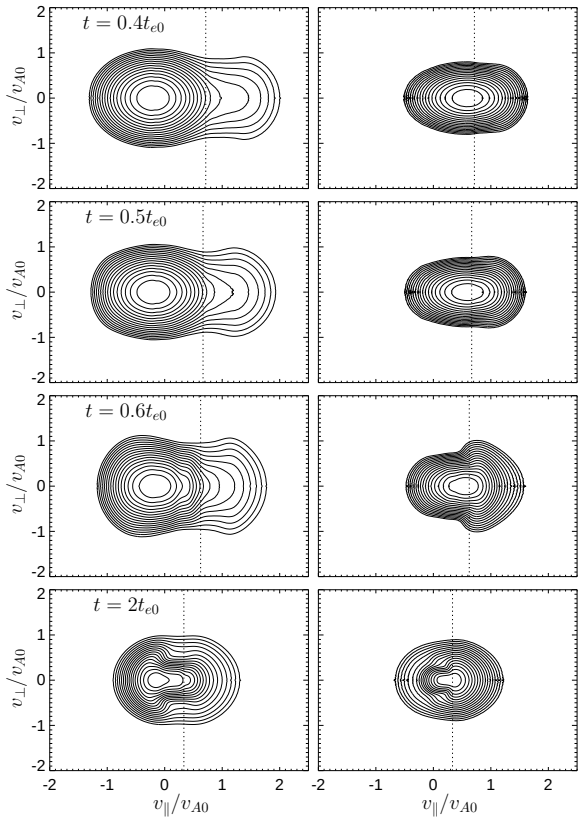

Figure 3. Ion velocity distribution functions as functions of $v_\parallel$ and $v_\perp$ (normalized to the initial Alfvén velocity v_{A0}) at (top panels) $t = 0.4t_{e0}$, (middle upper panels) $t = 0.5t_{e0}$, (middle lower panels) $t = 0.6t_{e0}$ and (bottom panels) at $t = 2t_{e0}$. Left panels show the total proton distribution functions, while right panels shows the alpha particle distribution functions. Dashed lines displays the local Alfvén velocity v_A.

Figure 3 shows that the general effect of the expansion, the perpendicular cooling which is partly counteracted by wave-particle interactions. The quasi-parallel waves interact mainly with the beam protons, slowing them and scattering them in the perpendicular direction. Alpha particles are only weakly affected by these waves. On the contrary, the transient oblique waves strongly influence the (resonant) alpha particles; they are decelerated and heated in the perpendicular direction. The beam protons likely interact with the oblique waves as well and the core protons are clearly heated in the perpendicular direction. These results are consistent with the quasi-linear predictions for the parallel magnetosonic and oblique Alfvén instabilities for the standard and anomalous cyclotron resonances (see Paper 1). Furthermore, there are indications of a formation of a quasi-linear plateau in the proton velocity distribution function due to the Landau resonance.

In order to discern the instabilities responsible for the wave generation we used the local ion velocity distribution functions and calculated the linear prediction, the maximum growth rate, as a function of time (when it was possible). The results of these calculations are shown in Figure 4 where dots displays the maximum linear growth rate calculated from the local/instantaneous ion velocity distribution functions as a function of time (see Paper 1). The top panel shows the maximum linear growth rate for the parallel magnetosonic instability, the middle panel shows the maximum linear growth rate for the oblique Alfvén instability and the bottom panel the maximum linear growth rate for the parallel proton cyclotron

instability for the propagation along the beam/alpha particles. For comparison we calculated temperatures and mean velocities of particles which initially formed the three populations and we calculated the maximum growth rate assuming bi-Maxwellian velocity distribution function for the three populations.

Figure 4 shows that the system becomes first unstable with respect the parallel magnetosonic instability, later on the oblique Alfvén instability appear but is rapidly stabilized which likely causes a stabilization of the parallel magnetosonic instability. Their interaction leads to an overall decrease of the fluctuating magnetic energy. The linear analysis indicates that after the stabilization the parallel magnetosonic instability becomes again weakly unstable and possibly the proton cyclotron instability gets weakly unstable. The linear prediction based on the assumption of bi-Maxwellian particles gives generally different maximum growth rates compared to the prediction based on the local velocity distribution functions; only initially when the particle velocity distribution functions remain close to bi-Maxwellian ones the two predictions give similar results. The maximum growth rate for the oblique Alfvén instability appear to reach much larger values that that of the other instabilities. This may possibility due to small volume of the unstable region (in the wavevector space) as indicated by the observed wave spectra at the oblique propagation. The important changes in the alpha particle velocity distribution function due to the interaction with oblique Alfvén waves indicate that the main source of the free energy for the oblique Alfvén instability is the differential velocity between alpha particles and core protons.

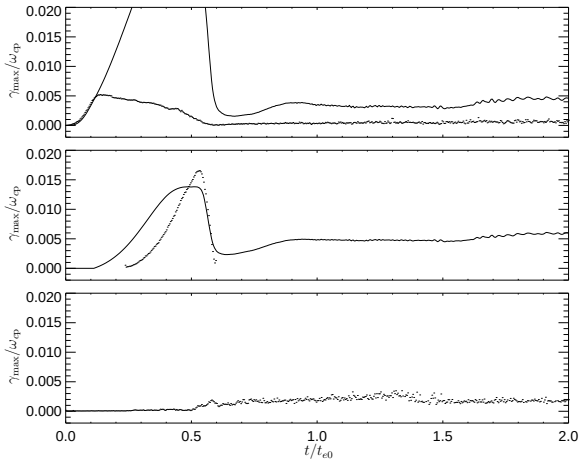

Figure 4. Dots denotes the maximum growth rate $\gamma_{\max}$ as a function of time for the relevant instabilities: (top) the parallel magnetosonic/fire hose instability for the propagation along the beam, (middle) oblique Alfvén instability, and (bottom) parallel proton cyclotron instability for the propagation along the beam (and the alpha particles). For comparison the solid lines show the linear prediction assuming bi-Maxwellian velocity distribution function for all three populations.

The complex evolution of ion velocity distribution functions (Figure 3) needs a further analysis. Here we try to characterize the two proton populations by fitting the proton velocity distribution function as a superposition of two bi-Maxwellian distributions drifting with respect to each other along the ambient magnetic field. We expect that such a fit would work at least at the beginning of the simulation as the initial velocity distribution function has this form.

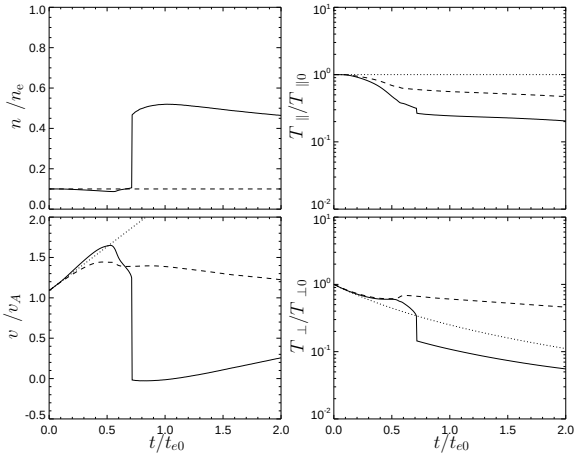

Figure 5. Evolution of the beam: (top left) number density, $n_{\rm b}$, (bottom left) mean velocity, $v_{\rm b}$, (top right) parallel, and (bottom right) perpendicular temperatures, $T_{\rm b\parallel}$ and $T_{\rm b\perp}$, as functions of time. Solid lines show results of a fit of the total proton distribution function as a sum of two bi-Maxwellian velocity distribution functions. Dashed lines show the moments calculated from protons which initially formed the beam. Dotted lines denote the double-adiabatic prediction.

Figure 5 shows the evolution of the beam properties obtained from the fit (solid lines) compared to the moments calculated from protons which initially formed the beam (dashed lines). Figure 5 displays (top left) number density, $n_{\rm b}$, (bottom left) mean velocity, $v_{\rm b}$, (top right) parallel, and (bottom right) perpendicular temperatures, $T_{\rm b\parallel}$ and $T_{\rm b\perp}$, as functions of time. For a comparison the dotted lines denote the double-adiabatic prediction. Figure 5 shows that initially the fit and the moments give similar results following the double adiabatic prediction. As an important wave activity develops the double adiabatic prediction is broken, beam protons are accelerated and heated in the perpendicular direction while they cool in the parallel directions. During this time the fitted results departs considerably from the calculated moments and after $t \gtrsim 0.7t_{e0}$ there is a jump in the fitted results which indicates that the proton velocity distribution cannot be at later times characterized as a superposition of two bi-Maxwellian distributions (see Figure 3).

Figure 6 shows the corresponding plot for the evolution of the core obtained from the fit (solid lines) compared to the moments calculated from protons which initially formed the beam (dashed lines). Figure 6 shows (top left) number density, $n_{\rm b}$, (bottom left) mean velocity, $v_{\rm p}$, (top right) parallel, and (bottom right) perpendicular temperatures, $T_{\rm p\parallel}$ and $T_{\rm p\perp}$, as functions of time in the same format as in Figure 5. For comparison the dotted lines denote the double-adiabatic prediction. Figure 6 shows that initially the fit and the moments give similar results and follow the double adiabatic prediction. As the important wave activity appears the core protons are weakly accelerated, cooled in the parallel direction and heated in the perpendicular one. The fitted results then departs considerably from the calculated moments and after $t \gtrsim 0.7t_{e0}$, there is the jump in the fitted results.

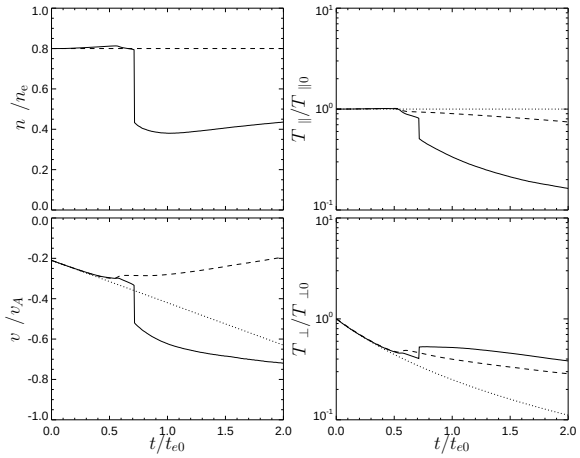

Figure 6. Evolution of the proton core: (top left) number density, n_b, (bottom left) mean velocity, v_p, (top right) parallel, and (bottom right) perpendicular temperatures, $T_{\mathrm{p}\parallel}$ and $T_{\mathrm{p}\perp}$, as functions of time. Solid lines show results of a fit of the total proton distribution function as a sum of two bi-Maxwellian velocity distribution functions. Dashed lines show the moments calculated from protons which initially formed the core. Dotted lines denote the double-adiabatic prediction.

The velocity distribution function of alpha particles also becomes quite complex during the simulation (see Figure 3). For comparison with the analysis of the proton velocity distribution function we have fitted the alpha particle distribution by one bi-Maxwellian distribution (although at later times the alpha particle distribution might be better characterized by two bi-Maxwellian populations). The results are shown in Fig. 7 which shows alpha particle number density, mean velocity and parallel and perpendicular temperatures as function of time. Solid lines show the results of the fit by a bi-Maxwellian velocity distribution function. Dashed lines show the moments calculated from the alpha particle velocity distribution function. Dotted lines denote the double-adiabatic prediction. The fitting procedure gives a good alpha particle number density. At later times there are clear discrepancies between the fitted moments and the moments calculated from the velocity distribution function. The fitted and calculated moments follow initially the double adiabatic prediction till $t \sim 0.5 t_{e0}$ when the oblique waves appear. The oblique waves seem to disrupt the double adiabatic behaviour, the alpha particles are importantly decelerated, cooled in the parallel direction and heated in the perpendicular direction.

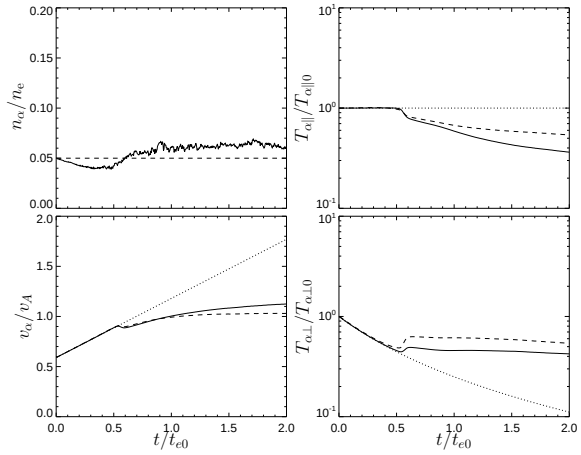

Figure 7. Evolution of the alpha particles: (top left) number density, n_α, (bottom left) mean velocity, v_α, (top right) parallel, and (bottom right) perpendicular temperatures, $T_{\alpha\parallel}$ and $T_{\alpha\perp}$, as functions of time. Solid lines show results of a fit of the alpha particle distribution function as a bi-Maxwellian velocity distribution function. Dashed lines show the moments calculated from the alpha particle velocity distribution function. Dotted lines denote the double-adiabatic prediction.

2.3. Temperatures and heating rates

From the macroscopic point of view it is interesting to investigate the properties of the total (effective) proton and alpha particle temperatures. Figure 8 shows the evolution of the total proton temperature (including the core and the beam and taking into account their differential velocity) in the top panel whereas the middle panel shows the evolution of the total alpha particle temperature. The bottom panel shows the ratio between the total alpha particle and proton temperatures (solid line); the dashed line shows the ratio between the total alpha particle and the core proton temperatures. The total proton temperature decreases faster than that of alpha particles. The nonlinear evolution of the system leads to a differential heating of protons and alpha particles, the ratio between the alpha particle and proton temperatures T_α/T_p increases with time.

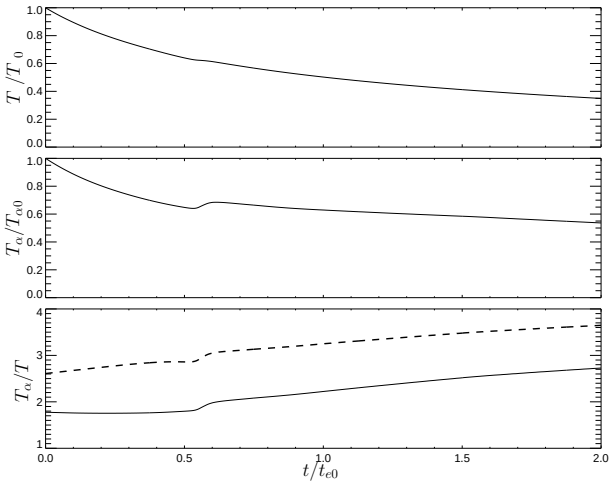

Figure 8. Evolution ion temperatures: (top) total (effective) proton temperature T_p, (middle) alpha particle temperature T_α , and (bottom) the ratio between the alpha particle temperature and the proton one (solid line) as functions of time. The dashed line on the bottom panel shows the ratio between the alpha particle temperature the total proton core temperature.

For the comparison with observations [*Hellinger et al.*, 2011, 2013] it is interesting to calculate ion heating rates. The heating rates are calculated as the difference between the actual temporal change of the spatially averaged ion temperatures and the double adiabatic (CGL) prediction

$$Q_{\mathrm{s}\parallel} = n_\mathrm{s} k_B \left[\frac{\mathrm{d}T_{\mathrm{s}\parallel}}{\mathrm{d}t} - \left(\frac{\mathrm{d}T_{\mathrm{s}\parallel}}{\mathrm{d}t} \right)_{CGL} \right]$$
$$Q_{\mathrm{s}\perp} = n_\mathrm{s} k_B \left[\frac{\mathrm{d}T_{\mathrm{s}\perp}}{\mathrm{d}t} - \left(\frac{\mathrm{d}T_{\mathrm{s}\perp}}{\mathrm{d}t} \right)_{CGL} \right]. \quad (8)$$

Figure 9 displays the evolution of the proton heating rates calculated from Equation (8) normalized to the dimensional heating rate $Q_E = nk_B T_\mathrm{p}/t_e$ (see Equation (1). Top panel shows the parallel heating rate $Q_{\mathrm{p}\parallel}$, the middle panels shows the perpendicular heating rate $Q_{\mathrm{p}\perp}$, and the bottom panel shows the average heating rate Q_p as functions of time. During the initial, double adiabatic phase there is no proton heating/cooling. When quasi-parallel waves appear, the protons are cooled in the parallel direction and heated in the perpendicular one; in total the proton are cooled as a part of their energy is transfered to the waves. The appearance of the oblique waves leads to transient and much stronger parallel cooling and perpendicular heating compared to the earlier times. At the same time the protons are shortly strongly heated (with the peak value about $0.4Q_E$). At later times the protons exhibit a steady parallel cooling and perpendicular heating, and, the protons are heated (in total) with a heating rate about $0.1Q_E$.

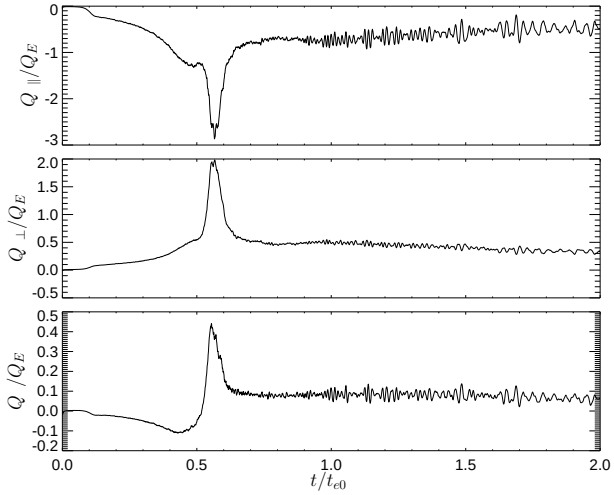

Figure 9. Estimated proton heating rates: (top) the parallel heating rate $Q_{\mathrm{p}\parallel}$, (middle) the perpendicular heating rate $Q_{\mathrm{p}\perp}$, and (bottom) the average heating rate Q_p normalized to Q_E as functions of time.

As in the case of protons we calculated the alpha particle heating rates. Figure 10 displays the evolution of the alpha particle heating rates normalized to Q_E. Top panel shows the parallel heating rate $Q_{\alpha\parallel}$, the middle panels shows the perpendicular heating rate $Q_{\alpha\perp}$, and the bottom panel shows the average heating rate Q_α as functions of time.

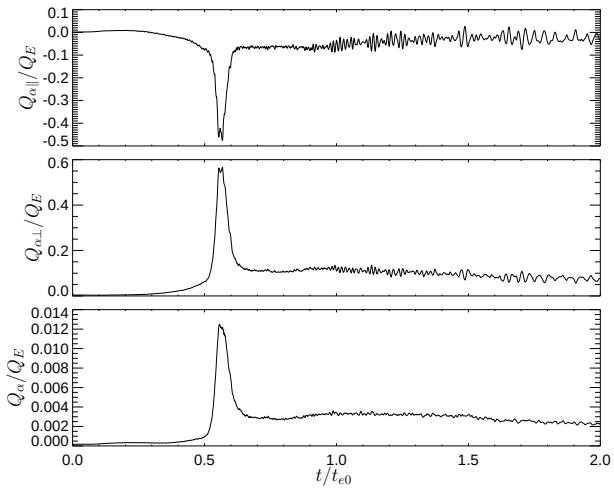

Figure 10. Estimated heating rates of alpha particles: (top) the parallel heating rate $Q_{\alpha\parallel}$, (middle) the perpendicular heating rate $Q_{\alpha\perp}$, and (bottom) the average heating rate Q_α normalized to the heating rate Q_E as functions of time.

The alpha particle are not very affected by the quasi-parallel waves. As the oblique waves appear the alpha particles exhibit a behavior qualitatively similar to that of protons. Alpha particles are transiently strongly cooled in the parallel direction and heated in the perpendicular one. At later times the alpha particles are weakly cooled in the parallel direction and heated in the perpendicular one; in total they are heated with a heating rate about $0.002Q_E$. The

heating rates of alphas are weaker than that of protons due to their much lower abundance; actually, the alpha particle temperature increases with time with respect to the proton one (see Figure 8).

3. Discussion

In this paper we presented results of the hybrid expanding box simulation of the plasma system consisting of proton core and beam populations, and of alpha particles (and of fluid massless electrons) drifting with respect to each other along the ambient magnetic field as typically observed in the solar wind.

The expansion drives the initially stable system unstable, first with respect to the parallel magnetosonic instability (due to the differential velocity between the beam and the core) and then with respect to the oblique Alfvén instability (mainly due to the differential velocity between the alpha particles and the core protons). The proton beam and the alpha particles are decelerated with respect to the core protons, heated in the perpendicular direction and cooled in the parallel one. There are indications that the perpendicular heating may at later times lead to a proton cyclotron instability driven by the anisotropic core protons. These results are in a qualitative agreement with Helios observations showing a continuous deceleration of the proton beam and alpha particle populations with respect to the core protons following the local Alfvén velocity.

The wave-particle interactions due to the driven instabilities lead to large departures of the ion velocity distribution functions from bi-Maxwellian shapes. Assuming bi-Maxwellian velocity distribution functions for proton core, beam and alpha particles is generally insufficient description of the ion velocity distribution functions; especially, the linear analysis based on the bi-Maxwellian distribution functions gives often quite different results compared with the analysis based on the instantaneous velocity distribution functions.

The evolution in the present simulated system is similar to that observed in the simulated proton beam-core system without alpha particles in Paper 1. The main difference is that the presence of the drifting alpha particles leads to a stronger oblique Alfvén instability (which is in this case driven by the alpha particles); consequently a part of the alpha-particle kinetic energy is transfered to protons. The proton parallel and perpendicular heating/cooling rates in the simulation are comparable to the heating rates estimated from the Helios observations around 0.3 AU [*Hellinger et al.*, 2011, 2013] Moreover, the total proton heating rate in the simulation reaches transiently values comparable with what is estimated from the Helios observations and at later times we observe a steady total proton heating which makes an important fraction of the observed proton heating rates in Helios data.

In the hybrid expanding box simulation alpha particles are cooled in the parallel direction and heated in the perpendicular one. The heating rates of alpha particles are weaker than those of protons but due to their smaller abundance the ratio between the alpha particle and proton temperatures increases with time; interestingly this is at odds with observations by *Marsch et al.* [1982a] who reported an overall decrease of the alpha particle to proton temperature ratio with the radial distance in contrast with the Ulysses observations in the high-latitude fast solar wind [*Reisenfeld et al.*, 2001] where the alpha particle to proton temperature ratio increases with the distance. Further analysis of Helios data is needed. The anisotropic thermal energetics of the alpha particles in the solar wind has not yet been investigated but from the radial profiles of the alpha particle parallel and perpendicular temperatures observed by Helios we expect that parallel cooling and perpendicular heating of alpha particles also occur in the inner heliosphere as observed in the high-latitude fast solar wind [*Reisenfeld et al.*, 2001].

The results of present and previous hybrid expanding box simulations show that there are many different kinetic processes that may influence temperatures of protons and alpha particles and their relative velocity on the way from the solar corona which should be taken into account when interpreting observed trends and correlations between different plasma parameters at 1 AU [*Gary et al.*, 2002; *Kasper et al.*, 2008, 2013]. The hybrid expanding model used in this paper does not fully describe the complex properties of the solar wind. The strictly radial magnetic field is assumed, the chosen characteristic expansion time is about ten times faster than in the solar wind and the model does not include any turbulence/wave activity typically present in the solar wind. The model, however, self-consistently resolves the competition between the expansion and kinetic ion instabilities. The simulation results suggest that the kinetic instabilities are partly responsible for the proton perpendicular heating and parallel cooling in the fast solar wind as observed by Helios. The simulation results also indicate that alpha particles play an important role in the solar wind ion energetics. A nonnegligible part of the necessary proton heating may be due the deceleration of alpha particles with respect to protons leading to an important total proton heating (a fraction of Q_E). We think that the effects of the proton beam and alpha particles populations observed in kinetic simulations need to be taken into account (especially the proton parallel cooling) when incorporating kinetic effects in fluid models of the solar wind [cf., *Chandran et al.*, 2011]. Further analyses of observed and simulated data are needed to determine quantitative roles of kinetic processes for ion energetics as well as for the evolution of ion velocity distribution functions.

Glossary

Here subscripts $\perp$ and $\parallel$ denote the perpendicular and parallel directions with respect to the ambient magnetic field $\boldsymbol{B}_0$, $B_0 = |\boldsymbol{B}_0|$ denotes its the magnitude; $\boldsymbol{v}$ denotes a velocity, $v = |\boldsymbol{v}|$ being its magnitude, and $v_\parallel$ and $v_\perp$ denote magnitude of the velocity components parallel and perpendicular to $\boldsymbol{B}_0$, respectively; t denotes the time. Here R denotes the radial distance from the sun, v_{sw} denote the solar wind velocity and $t_e = R/v_{sw}$ is the expansion time. Here subscript s (and s') denotes different species (e: electrons, c: core protons, b: beam protons, p stands for all the protons, α denotes alpha particles); subscript 0 denotes initial values. Here n_s denotes the number density, v_s denotes the mean parallel velocities, and $v_{\mathrm{ss}'} = v_\mathrm{s} - v_{\mathrm{s}'}$ denotes the relative parallel velocity between species s and s'. Here $T_{\mathrm{s}\parallel}$ and $T_{\mathrm{s}\perp}$ denote the parallel and perpendicular temperatures, respectively, $T_\mathrm{s} = (2T_{\mathrm{s}\perp} + T_{\mathrm{s}\parallel})/3$ is the mean temperature of species s. Here $\beta_{\mathrm{s}\parallel} = 2\mu_0 n_\mathrm{s} k_B T_{\mathrm{s}\parallel}/B_0^2$ is the parallel beta, $\omega_{c\mathrm{s}} = q_\mathrm{s} B_0/m_\mathrm{s}$ and $\omega_{p\mathrm{s}} = \left(n_\mathrm{s} q_\mathrm{s}^2/m_\mathrm{s}\epsilon_0\right)^{1/2}$ denote the cyclotron and plasma frequencies, respectively. In these expressions m_s denotes the mass, k_B is the Boltzmann constant, q_s denotes the charge, ϵ_0 and μ_0 denote the vacuum electric permittivity and magnetic permeability, respectively. Here v_A denotes the Alfvén velocity $v_A = B_0/(\mu_0 m_\mathrm{p} n_\mathrm{e})^{1/2}$ and c denotes the speed of light. Here, $\boldsymbol{k}$ denotes the wave vector, k its magnitude, $k_\parallel$ and $k_\perp$ its parallel and perpendicular components, respectively, θ_{kB} denotes the angle between $\boldsymbol{k}$ and the ambient magnetic field.

Acknowledgments. Authors acknowledge the grant P209/12/2023 of the Grant Agency of the Czech Republic. The research leading to these results has received funding from the European Commission's Seventh Framework Programme (FP7) under the grant agreement SHOCK (project number 284515, http://project-shock.eu).

References

Bale, S. D., J. C. Kasper, G. G. Howes, E. Quataert, C. Salem, and D. Sundkvist (2009), Magnetic fluctuation power near proton temperature anisotropy instability thresholds in the solar wind, *Phys. Rev. Lett.*, *103*, 211101.

Chandran, B. D. G., T. J. Dennis, E. Quataert, and S. D. Bale (2011), Incorporating kinetic physics into a two-fluid solar-wind model with temperature anisotropy and low-frequency Alfvén-wave turbulence, *Astrophys. J.*, *743*, 197, doi:10.1088/0004-637X/743/2/197.

Daughton, W., and S. P. Gary (1998), Electromagnetic proton/proton instabilities in the solar wind, *J. Geophys. Res.*, *103*, 20,613–20,620.

Daughton, W., S. P. Gary, and D. Winske (1999), Electromagnetic proton/proton instabilities in the solar wind: Simulations, *J. Geophys. Res.*, *104*, 4657–4668.

Gary, S. P., R. M. Skoug, J. T. Steinberg, and C. W. Smith (2001), Proton temperature anisotropy constraint in the solar wind: ACE observations, *Geophys. Res. Lett.*, *28*, 2759–2763.

Gary, S. P., B. E. Goldstein, and M. Neugebauer (2002), Signatures of wave-ion interactions in the solar wind: Ulysses observations, *J. Geophys. Res.*, *107*, 1169, doi:10.1029/2001JA000269.

Goldstein, B. E., M. Neugebauer, L. D. Zhang, and S. P. Gary (2000), Observed constraint on proton-proton relative velocities in the solar wind, *Geophys. Res. Lett.*, *27*, 53–56.

Hellinger, P., and P. Trávníček (2005), Magnetosheath compression: Role of characteristic compression time, alpha particle abundances and alpha/proton relative velocity, *J. Geophys. Res.*, *110*, A04210, doi: 10.1029/2004JA010687.

Hellinger, P., and P. Trávníček (2008), Oblique proton fire hose instability in the expanding solar wind: Hybrid simulations, *J. Geophys. Res.*, *113*, A10109, doi:10.1029/2008JA013416.

Hellinger, P., and P. M. Trávníček (2011), Proton core-beam system in the expanding solar wind: Hybrid simulations, *J. Geophys. Res.*, *116*, A11101, doi:10.1029/2011JA016940.

Hellinger, P., P. Trávníček, A. Mangeney, and R. Grappin (2003), Hybrid simulations of the expanding solar wind: Temperatures and drift velocities, *Geophys. Res. Lett.*, *30*, 1211, doi:10.1029/2002GL016409.

Hellinger, P., M. Velli, P. Trávníček, S. P. Gary, B. E. Goldstein, and P. C. Liewer (2005), Alfvén wave heating of heavy ions in the expanding solar wind: Hybrid simulations, *J. Geophys. Res.*, *110*, A12109, doi: 10.1029/2005JA011244.

Hellinger, P., P. Trávníček, J. C. Kasper, and A. J. Lazarus (2006), Solar wind proton temperature anisotropy: Linear theory and WIND/SWE observations, *Geophys. Res. Lett.*, *33*, L09101, doi: 10.1029/2006GL025925.

Hellinger, P., L. Matteini, Š. Štverák, P. M. Trávníček, and E. Marsch (2011), Heating and cooling of protons in the fast solar wind between 0.3 and 1 AU: Helios revisited, *J. Geophys. Res.*, *116*, A09105, doi: 10.1029/2011JA016674.

Hellinger, P., P. M. Trávníček, Š. Štverák, L. Matteini, and M. Velli (2013), Proton thermal energetics in the solar wind: Helios reloaded, *J. Geophys. Res.*, *118*, 1351–1365, doi:10.1002/jgra.50107.

Hollweg, J. V., and P. A. Isenberg (1981), On rotational forces in the solar wind, *J. Geophys. Res.*, *86*, 11,463.

Kasper, J. C., A. J. Lazarus, and S. P. Gary (2008), Hot solar-wind helium: Direct evidence for local heating by Alfvén-cyclotron dissipation, *Phys. Rev. Lett.*, *101*, 261103.

Kasper, J. C., B. A. Maruca, M. L. Stevens, and A. Zaslavsky (2013), Sensitive test for ion-cyclotron resonant heating in the solar wind, *Phys. Rev. Lett.*, *110*, 091102, doi:10.1103/PhysRevLett.110.091102.

Li, B., S. R. Habbal, and X. Li (2007), Angular momentum transport and proton-alpha-particle differential streaming in the solar wind, *Astrophys. J.*, *661*, 593–601.

Liewer, P. C., M. Velli, and B. E. Goldstein (2001), Alfvén wave propagation and ion cyclotron interaction in the expanding solar wind: One-dimensional hybrid simulations, *J. Geophys. Res.*, *106*, 29,261–29,281.

MacBride, B. T., C. W. Smith, and M. A. Forman (2008), The turbulent cascade at 1 AU: Energy transfer and the third-order scaling for MHD, *Astrophys. J.*, *679*, 1644–1660.

Marsch, E., and S. Livi (1987), Observational evidence for marginal stability of solar wind ion beams, *J. Geophys. Res.*, *92*, 7263–7268.

Marsch, E., K. H. Muhlhauser, H. Rosenbauer, R. Schwenn, and F. M. Neubauer (1982a), Solar wind helium ions: Observations of the Helios solar probes between 0.3 AU and 1 AU, *J. Geophys. Res.*, *87*, 35–51.

Marsch, E., K. H. Muhlhauser, R. Schwenn, H. Rosenbauer, W. Pilipp, and F. M. Neubauer (1982b), Solar wind protons: Three-dimensional velocity distributions and derived plasma parameters measured between 0.3 AU and 1 AU, *J. Geophys. Res.*, *87*, 52–72.

Maruca, B. A., J. C. Kasper, and S. P. Gary (2012), Instability-driven limits on Helium temperature anisotropy in the solar wind: Observations and linear Vlasov analysis, *Astrophys. J.*, *748*, 137, doi:10.1088/0004-637X/748/2/137.

Matteini, L., S. Landi, P. Hellinger, and M. Velli (2006), Parallel proton fire hose instability in the expanding solar wind: Hybrid simulations, *J. Geophys. Res.*, *111*, A10101, doi:10.1029/2006JA011667.

Matteini, L., S. Landi, P. Hellinger, F. Pantellini, M. Maksimovic, M. Velli, B. E. Goldstein, and E. Marsch (2007), The evolution of the solar wind proton temperature anisotropy from 0.3 to 2 AU, *Geophys. Res. Lett.*, *34*, L20105, doi:10.1029/2007GL030920.

Matteini, L., P. Hellinger, S. Landi, P. M. Trávníček, and M. Velli (2012), Ion kinetics in the solar wind: coupling global expansion to local microphysics, *Space Sci. Rev.*, *172*, 373–396, doi:10.1007/s11214-011-9774-z.

Matteini, L., P. Hellinger, B. E. Goldstein, S. Landi, M. Velli, and M. Neugebauer (2013), Signatures of kinetic instabilities in the solar wind, *J. Geophys. Res.*, *118*, 2771–2782, doi:10.1002/jgra.50320.

Matthaeus, W. H., and M. Velli (2011), Who needs turbulence? A review of turbulence effects in the heliosphere and on the fundamental process of reconnection, *Space Sci. Rev.*, *160*, 145–168, doi:10.1007/s11214-011-9793-9.

Matthews, A. (1994), Current advance method and cyclic leapfrog for 2D multispecies hybrid plasma simulations, *J. Comput. Phys.*, *112*, 102–116.

McKenzie, J. F., W.-H. Ip, and W. I. Axford (1979), The acceleration of minor ion species in the solar wind, *Astrophys. Space Sci.*, *64*, 183–211.

Neugebauer, M. (1976), The role of Coulomb collisions in limiting differential flow and temperature differences in the solar wind, *J. Geophys. Res.*, *81*, 78–82.

Reisenfeld, D. B., S. P. Gary, J. T. Gosling, J. T. Steinberg, D. J. McComas, B. E. Goldstein, and M. Neugebauer (2001), Helium energetics in the high-latitude solar wind: Ulysses observations, *J. Geophys. Res.*, *106*, 5693–5708.

Schwartz, S. J., and E. Marsch (1983), The radial evolution of a single solar wind plasma parcel, *J. Geophys. Res.*, *88*, 9919–9932.

Schwartz, S. J., W. C. Feldman, and S. P. Gary (1981), The source of proton anisotropy in the high-speed solar wind, *J. Geophys. Res.*, *86*, 541–546.

Tu, C.-Y., E. Marsch, and Z.-R. Qin (2004), Dependence of the proton beam drift velocity on the proton core plasma beta in the solar wind, *J. Geophys. Res.*, *109*, A05101, doi:10.1029/2004JA010391.

Vasquez, B. J., C. W. Smith, K. Hamilton, B. T. MacBride, and R. J. Leamon (2007), Evaluation of the turbulent energy cascade rates from the upper inertial range in the solar wind at 1 AU, *J. Geophys. Res.*, *112*, A07101, doi:10.1029/2007JA012305.

Verscharen, D., S. Bourouaine, and B. D. G. Chandran (2013), Instabilities driven by the drift and temperature anisotropy of alpha particles in the solar wind, *Astrophys. J.*, *773*, 163.

P. Hellinger, Astronomical Institute, AS CR, Prague 14100, Czech Republic. (petr.hellinger@asu.cas.cz)

P. M. Trávníček, Space Sciences Laboratory, UCB, Berkeley, USA. (pavel@ssl.berkeley.edu)